HHS Public Access

Author manuscript

Phys Rev Lett. Author manuscript; available in PMC 2016 September 04.

Published in final edited form as:

Phys Rev Lett. 2016 March 4; 116(9): 098101. doi:10.1103/PhysRevLett.116.098101.

Emergent collective chemotaxis without single-cell gradient sensing

Brian A. Camley[1], **Juliane Zimmermann**[2], **Herbert Levine**[2,3], and **Wouter-Jan Rappel**[1]

[1]Department of Physics, University of California, San Diego, La Jolla CA 92093

[2]Center for Theoretical Biological Physics, Rice University, Houston, TX

[3]Department of Bioengineering, Rice University, Houston, TX

Abstract

Many eukaryotic cells chemotax, sensing and following chemical gradients. However, experiments have shown that even under conditions when single cells cannot chemotax, small clusters may still follow a gradient. This behavior has been observed in neural crest cells, in lymphocytes, and during border cell migration in Drosophila, but its origin remains puzzling. Here, we propose a new mechanism underlying this “collective guidance”, and study a model based on this mechanism both analytically and computationally. Our approach posits that contact inhibition of locomotion (CIL), where cells polarize away from cell-cell contact, is regulated by the chemoattractant. Individual cells must measure the mean attractant value, but need not measure its gradient, to give rise to directional motility for a cell cluster. We present analytic formulas for how cluster velocity and chemotactic index depend on the number and organization of cells in the cluster. The presence of strong orientation effects provides a simple test for our theory of collective guidance.

Cells often perform chemotaxis, detecting and moving toward increasing concentrations of a chemoattractant, to find nutrients or reach a targeted location. This is a fundamental aspect of biological processes from immune response to development. Many single eukaryotic cells sense gradients by measuring how a chemoattractant varies over their length [1]; this is distinct from bacteria that measure chemoattractant over time [2]. In both, single cells have a net motion toward higher chemoattractant.

Recent measurements of how neural crest cells respond to the chemoattractant Sdf1 suggest that single neural crest cells cannot chemotax effectively, but small clusters can [3]. A more recent report shows that at low gradients, clusters of lymphocytes also chemotax without corresponding single cell directional behavior; at higher gradients clusters actually move oppositely to single cells [4]. Late border cell migration in the *Drosophila* egg chamber may also occur by a similar mechanism [5–8]. These experiments strongly suggest that gradient sensing in a cluster of cells may be an *emergent* property of cell-cell interactions, rather than arising from amplifying a single cell’s biased motion; interestingly, some fish schools also display emergent gradient sensing [9]. In fact, these experiments led to a “collective guidance” hypothesis [6], in which a cluster of cells where each individual cell has no information about the gradient may nevertheless move directionally. In a sense that will

become clear, cell-cell interactions allow for a measurement of the gradient across the entire cluster, as opposed to across a single cell.

In this paper, we develop a quantitative model that embodies the collective guidance hypothesis. Our model is based on modulation of the well-known contact inhibition of locomotion (CIL) interaction [10–12], in which cells move away from neighboring cells. We propose that individual cells measure the local signal concentration and adjust their CIL strength accordingly; the cluster moves directionally due to the spatial bias in the cell-cell interaction. We discuss the suitability of this approach for explaining current experiments, and provide experimental criteria to distinguish between chemotaxis via collective guidance and other mechanisms where clusters could gain improvement over single-cell migration [13, 14]. These results may have relevance to collective cancer motility [15], as recent data suggest that tumor cell clusters are particularly effective metastatic agents [16].

We consider a cluster of cells exposed to a chemical gradient $S(\mathbf{r})$. We use a two-dimensional stochastic particle model to describe cells, giving each cell i a position $\mathbf{r}^i$ and a polarity $\mathbf{p}^i$. The cell polarity indicates its direction and propulsion strength: an isolated cell with polarity $\mathbf{p}^i$ has velocity $\mathbf{p}^i$. The cell's motion is overdamped, so the cell's velocity is $\mathbf{p}^i$ plus the total physical force other cells exert on it, $\sum_{j\neq i}\mathbf{F}^{ij}$. Biochemical interaction between cells alter a cell's polarity $\mathbf{p}^i$. Our model is then:

$$\partial_t \mathbf{r}^i = \mathbf{p}^i + \sum_{j\neq i} \mathbf{F}^{ij} \quad (1)$$

$$\partial_t \mathbf{p}^i = -\frac{1}{\tau}\mathbf{p}^i + \sigma\boldsymbol{\xi}^i(t) + \beta^i \sum_{j\sim i} \hat{\mathbf{r}}^{ij} \quad (2)$$

where $\mathbf{F}^{ij}$ are intercellular forces of cell-cell adhesion and volume exclusion, and $\boldsymbol{\xi}^i(t)$ are Gaussian Langevin noises with $\langle \xi^i_\mu(t)\xi^j_\nu(t')\rangle = 2\delta_{\mu\nu}\delta^{ij}\delta(t-t')$. Greek indices μ, ν run over the dimensions *x, y*. The first two terms on the right of Eq. 2 are a standard Ornstein-Uhlenbeck model [17, 18]: $\mathbf{p}^i$ relaxes to zero with timescale τ, but is driven away from zero by the noise $\boldsymbol{\xi}(t)$. This corresponds with a cell that is orientationally persistent over time τ.

We introduce the last term in Eq. 2 to describe contact inhibition of locomotion (CIL). CIL is a well-known property of many cell types in which cells polarize away from cell-cell contact [11, 12, 19–21]. We model CIL by biasing $\mathbf{p}^i$ away from nearby cells, toward $\mathbf{q}^i = \sum_{j\sim i}\mathbf{r}^{\hat{ij}}$, where $\mathbf{r}^{\hat{ij}} = (\mathbf{r}^i - \mathbf{r}^j)/|\mathbf{r}^i - \mathbf{r}^j|$ is the unit vector pointing from cell j to cell i and the sum over $j \sim i$ indicates the sum over the neighbors of i (those cells within a distance $D_0 = 1.2$ cell diameters). While this is motivated by CIL in neural crest, it is also a natural minimal model under the assumption that cells know nothing about their neighbors other than their direction $\mathbf{r}^{\hat{ij}}$. For cells along the cluster edge, CIL bias $\mathbf{q}^i$ points outward, but for interior cells $\mathbf{q}^i$ is smaller or zero (Fig. 1a). This is consistent with experimental observations that edge cells have a strong outward polarity, while interior cells have weaker protrusions [3].

Chemotaxis arises in our model if the chemoattractant $S(\mathbf{r})$ changes a cell's susceptibility to CIL, β^i, $\beta^i = \beta\bar{S}(\mathbf{r}^i)$. This models the result of [3] that the chemoattractant Sdf1 stabilizes

protrusions induced by CIL [3]. We also assume the cell's chemotactic receptors are not close to saturation - i.e. the response is perfectly linear. If CIL occurs without chemoattractant ($S = 0$), as in neural crest [3], i.e. $\beta^i = \beta_0 + \beta\bar{S}(\mathbf{r})$, this will not significantly change our analysis, only shifting the strength of CIL at the origin. Similar results are obtained if all protrusions are stabilized by Sdf1 (τ regulated by S), though with complications (*Supplementary Information*, Fig. S1).

Analytic predictions for cluster velocity

Our model predicts that while single cells do not chemotax, clusters as small as two cells will, consistent with [3]. We can analytically predict the mean drift of a cluster of cells obeying Eqs. 1–2:

$$\langle \mathbf{V} \rangle_c \approx \overline{\beta}_\tau \mathscr{M} \cdot \nabla S \quad (3)$$

where the approximation is true for shallow gradients, $S(\mathbf{r}) \approx S_0 + \mathbf{r} \cdot \nabla S$. $\langle \cdots \rangle_c$ indicates an average over the fluctuating $\mathbf{p}^i$ but with a fixed configuration of cells $\mathbf{r}^i$. The matrix $\mathscr{M}$ only depends on the cells' configuration,

$$\mathscr{M}_{\mu\nu} = \frac{1}{N} \sum_i q_\mu^i r_\nu^i \quad (4)$$

where, as above, $\mathbf{q}^i = \sum_{j\sim i} \mathbf{r}^{\hat{ij}}$. Eq. 3 resembles the equation of motion for an arbitrarily shaped object in a low Reynolds number fluid under a constant force $\beta\bar{\tau}\nabla S$ [22]: by analogy, we call $\mathscr{M}$ the "mobility matrix." There is, however, no fluctuation-dissipation relationship as there would be in equilibrium [23].

To derive Eq. 3, we note that in our units, the velocity of a single cell is equal to the force on it, i.e. the mobility is one (Eq. 1). For a cluster of N cells, the mean velocity of the cluster is $1/N$ times the total force on the cluster. As $\mathbf{F}^{ij} = -\mathbf{F}^{ji}$, the cluster velocity is $\mathbf{V} = N^{-1} \sum_i \mathbf{p}^i$. When the cluster configuration changes slowly over timescale τ, Eq. 2 can be treated as an Ornstein-Uhlenbeck equation with a time-independent bias from CIL. The mean polarity is then $\langle \mathbf{p}^i \rangle = \beta^i \tau \sum_{j\sim i} \mathbf{r}^{\hat{ij}}$, with Gaussian fluctuations away from the mean, $\langle (\mathbf{p}_\mu^i - \langle \mathbf{p}_\mu^i \rangle)^2 \rangle = \sigma^2 \tau$. The mean cell cluster velocity is

$$\langle \mathbf{V} \rangle_c = \frac{\overline{\beta}_\tau}{N} \sum_i S(\mathbf{r}^i) \sum_{j\sim i} \hat{\mathbf{r}}^{ij} \quad (5)$$

In a constant chemoattractant field, $S = S_0$, no net motion is observed, as $\sum_i \sum_{j\sim i} \mathbf{r}^{\hat{ij}} = 0$. For linear or slowly-varying gradients $S(\mathbf{r}) \approx S_0 + \mathbf{r} \cdot \nabla S$, and we get Eq. 3.

Cluster motion and chemotactic efficiency depend on cluster size, shape, and orientation

Within our model, a cluster's motion can be highly anisotropic. Consider a pair of cells separated by unit distance along $(\cos\theta, \sin\theta)$. Then,

$\mathscr{M}_{xx}=\frac{1}{2}\cos^2\theta, \mathscr{M}_{xy}=\mathscr{M}_{yx}=\frac{1}{2}\cos\,\theta\,\sin\,\theta, \mathscr{M}_{yy}=\frac{1}{2}\sin^2\theta$. If the gradient is in the x direction, then $\langle V_x\rangle_c=\frac{V_0}{2}\cos^2\theta$ and $\langle V_y\rangle_c=\frac{V_0}{2}\cos\,\theta\,\sin\,\theta$, where $V_0 = \beta\bar{\tau}|\nabla S|$. Cell pairs move toward higher chemoattractant, but their motion is along the pair axis, leading to a transient bias in the y direction before the cell pair reorients due to fluctuations in $\mathbf{p}^i$ (Fig. 2). We compare our theory for the motility of rigid cell clusters (Eq. 3) with a simulation of Eq. 1–2 with strongly adherent cell pairs with excellent agreement (Fig. 2).

For the simulations in Fig. 2 and throughout the paper, we solve the model equations Eqs. 1–2 numerically using a standard Euler-Maruyama scheme. We choose units where the equilibrium cell-cell separation (roughly 20 μm for neural crest [3]) is unity, and the relaxation time $\tau = 1$ (we estimate $\tau = 20$ minutes in neural crest [3]). Within these units, neural crest cell velocities are on the order of 1. We choose $\sigma = 1$, so the root mean square speed of an isolated cell is $\langle|\mathbf{V}|^2\rangle^{1/2} = 2^{1/2}\,\sigma\tau^{1/2} \approx 1.4$ microns/minute. The cluster velocity scale is $V_0 = \beta\bar{\tau}|\nabla S|$, which is 0.5 (0.5 microns/minute in physical units) if $|\nabla S| = 0.025$ and $S(0) = 1$, i.e. β^i changes by 2.5% across a cell at the origin. Cell-cell forces $\mathbf{F}^{ij}$ are stiff springs so that clusters are effectively rigid (see *Supplementary Information* for details).

We can also compute $\mathscr{M}$ and hence $\langle V_x\rangle$ for larger clusters (Table S1, *Supplementary Information*, Fig. S2). For a cluster of Q layers of cells surrounding a center cell, $\mathscr{M}_{\mu\nu} = f(Q)\delta_{\mu\nu}$, with $f(Q)=\frac{9Q^2+3Q}{2+6Q+6Q^2}$. A cluster with Q layers has $N = 1 + 3Q + 3Q^2$ cells; thus the mean velocity of a Q-layer cluster is given by $\langle V_x\rangle/V_0=\overline{\mathscr{M}}=\frac{3N-\sqrt{12N-3}}{2N}$, where $\overline{\mathscr{M}}=\frac{1}{2}(\mathscr{M}_{xx}+\mathscr{M}_{yy})$ is the angular average of $\mathscr{M}$. We predict that $\langle V_x\rangle/V_0$ first increases with N, then slowly saturates to 3/2. This is confirmed by full model simulations (Fig. 3a). We note that $\langle V_x\rangle$ is an average over time, and hence orientation (see below, *Supplementary Information*). We can see why $\langle V_x\rangle$ saturates as $N\to\infty$ by considering a large circular cluster of radius R. Here, we expect $\mathbf{q}^i = a\hat{\mathbf{n}}$ on the outside edge, where a is a geometric prefactor and $\hat{\mathbf{n}}$ is the outward normal, with $\mathbf{q}^i = \mathbf{0}$ elsewhere. Then,

$\mathscr{M}_{\mu\nu}\sim\frac{a}{\pi R^2}\int_0^{2\pi}(Rd\theta)\hat{\mathbf{n}}_\mu(\theta)\mathbf{r}_\nu=2a\delta_{\mu\nu}$, independent of cluster radius R. A related result has been found for circular clusters by Malet-Engra et al. [4]; we note that they do not consider the behavior of single cells or cluster geometry.

The efficiency of cluster chemotaxis may be measured by chemotactic index (CI), commonly defined as the ratio of distance traveled along the gradient (the x displacement) to total distance traveled [24]; CI ranges from −1 to 1. We define $\mathrm{CI} \equiv \langle V_x\rangle/\langle|\mathbf{V}|\rangle$, where the average is over both time and trajectories (and hence over orientation). The chemotactic index CI may also be computed analytically, and it depends on the variance of $\mathbf{V}$, which is $\langle(V_x - \langle V_x\rangle)^2\rangle = \langle(V_y - \langle V_y\rangle)^2\rangle = \sigma^2\,\tau/N$. In our model, CI only depends on the ratio c of mean chemotactic velocity to its standard deviation,

$$\mathrm{CI}=\sqrt{2/\pi}c/L_{1/2}(-c^2/2)\ c=\frac{\langle V_x\rangle}{\sqrt{\langle(V_\mu-\langle V_\mu\rangle)^2\rangle}}=\frac{\overline{\beta}_\tau\overline{\mathscr{M}}|\nabla S|}{\sigma\sqrt{\tau/N}} \quad (6)$$

where $L_{1/2}$ is a generalized Laguerre polynomial. When mean cluster velocity is much larger than its fluctuations, $c \gg 1$ and CI $\to 1$, but when fluctuations are large, $|c| \ll 1$ and CI $\to 0$ (*Supplementary Information*, Fig. S3). Together, Eq. 3, Eq. 6 and Table S1 provide an analytic prediction for cluster velocity and CI, with excellent agreement with simulations (Fig. 3). We note that $\langle V_x\rangle/V_0$ only depends on cluster configuration, where $V_0 = \beta\bar{\tau}|\nabla S|$, so $\langle V_x(N)\rangle/V_0$ collapses onto a single curve as the gradient strength is changed (Fig. 3a). By contrast, how CI increases with N depends on $|\nabla S|$ and σ (Eq. 6, Fig. 3b).

In our model, clusters can in principle develop spontaneous rotation, but in practice this effect is small, and absent for symmetric clusters (see *Supplementary Information*).

Motion in non-rigid clusters

While we studied near-rigid clusters above, our results hold qualitatively for clusters that are loosely adherent and may rearrange. Cell rearrangements are common in many collective cell motions [25–28]. We choose cell-cell forces $\mathbf{F}^{ij}$ to allow clusters to rearrange (see *Supplementary Information*, [29]), and simulate Eqs. 1–2. As in rigid clusters, $\langle V_x\rangle$ increases and saturates, while CI increases toward unity, though more slowly than a rigid cluster (Fig. 4ab). Clusters may fragment; with increasing x, $\bar{\beta}^i$ increases and the cluster breaks up (Fig. 4c). Cluster breakup can limit guidance – if $\bar{\beta}$ is too large, clusters are not stable. We thus decreased $\bar{\beta}$ in Fig. 4.

In Fig. 4ab, we compute CI and velocity by averaging over all cells, not merely those that are connected. If we track cells ejected from the cluster, they have apparent CI > 0, as they are preferentially ejected from the high-$\bar{\beta}^i$ edge (*Supplementary Information*). Experimental analysis of dissociating clusters may therefore not be straight-forward. Anisotropic chemotaxis is present in non-rigid pairs, though lessened because they rotate quickly with respect to τ (*Supplementary Information*).

Distinguishing between potential collective chemotaxis models

Our model explains how chemotaxis can emerge from interactions of non-chemotaxing cells. However, other possibilities exist for enhancement of chemotaxis in clusters. Coburn et al. showed that in contact-based models, a few chemotactic cells can direct many non-chemotactic ones [14]. If single cells are weakly chemotactic, cell-cell interactions could amplify this response or average out fluctuations [13]. How can we distinguish these options? In lymphocytes [4], the motion of single cells oppositely to the cluster immediately rules out simple averaging or amplification of single cell bias. More generally, the scaling of collective chemotaxis with cluster size does not allow easy discrimination. In Fig. 3, at large N, $\langle V_x\rangle$ and CI saturate. As an alternate theory, suppose each cell chemotaxes noisily, e.g. $\mathbf{p}^i = p_0 \nabla S + \mathbf{\Delta}^i$, where $\mathbf{\Delta}$ are independent zero-mean noises. In this case, $\langle \mathbf{V}\rangle = p_0 \nabla S$ independent of N, and $\langle(V_\mu - \langle V_\mu\rangle)^2\rangle \sim 1/N$, as in our large-$N$ asymptotic results and the

related circular-cluster theory of [4]. Instead, we propose that orientation effects in small clusters are a good test of emergent chemotaxis. In particular, studying cell pairs as in Fig. 2 is critical: anisotropic chemotaxis is a generic sign of cluster-level gradient sensing. Even beyond our model, chemotactic drift is anisotropic for almost all mechanisms where single cells do not chemotax, because two cells separated per-pendicular to the gradient sense the same concentration. This leads to anisotropic chemotaxis unless cells integrate information over times much larger than the pair's reorientation time. By contrast, the simple model with single cell chemotaxis above leads to isotropic chemotaxis of pairs.

How well does our model fit current experiments? We find increasing cluster size increases cluster velocity and chemotactic index. This is consistent with [4], who see an increase in taxis from small clusters (< 20 cells) to large, but not [3], who find similar CI in small and large clusters, and note no large variations in velocity. This suggests the minimal version of collective guidance developed here can create chemotaxis, but does not fully explain the experiments of [3]. There are many directions for improvement. More quantitative comparisons could be made by detailed measurement of single-cell statistics [17, 30], leading to nonlinear or anisotropic terms in Eq. 2. Our description of CIL has also assumed, for simplicity, that both cell front and back are inhibitory; other possibilities may alter collective motility [20]. We could also add adaptation as in the LEGI model [31, 32], enabling clusters to adapt their response to a value independent of the mean chemoattractant concentration. We will treat extensions of this model elsewhere; our focus here is on the simplest possible results.

In summary, we provide a simple, quantitative model that embodies a minimal version of the collective guidance hypothesis [3, 6] and provides a plausible initial model for collective chemotaxis when single cells do not chemotax. Our work allows us to make an unambiguous and testable prediction for emergent collective guidance: pairs of cells have anisotropic chemotaxis. Although considerable effort has been devoted to models of collective motility [27, 33–41], ours is the first model of how collective chemotaxis can emerge from single non-gradient-sensing cells via collective guidance and regulation of CIL.

Supplementary Material

Refer to Web version on PubMed Central for supplementary material.

Acknowledgments

BAC appreciates helpful discussions with Albert Bae and Monica Skoge. This work was supported by NIH Grant No. P01 GM078586, NSF Grant No. DMS 1309542, and by the Center for Theoretical Biological Physics. BAC was supported by NIH Grant No. F32GM110983.

References

1. Levine H, Rappel W-J. Physics Today. 2013; 66
2. Segall JE, Block SM, Berg HC. Proceedings of the National Academy of Sciences. 1986; 83:8987.
3. Theveneau E, Marchant L, Kuriyama S, Gull M, Moepps B, Parsons M, Mayor R. Developmental Cell. 2010; 19:39. [PubMed: 20643349]

4. Malet-Engra G, Yu W, Oldani A, Rey-Barroso J, Gov NS, Scita G, Dupré L. Current Biology. 2015; 25:242. [PubMed: 25578904]
5. Bianco A, Poukkula M, Cliffe A, Mathieu J, Luque CM, Fulga TA, Rørth P. Nature. 2007; 448:362. [PubMed: 17637670]
6. Rørth P. Trends in Cell Biology. 2007; 17:575. [PubMed: 17996447]
7. Inaki M, Vishnu S, Cliffe A, Rørth P. Proceedings of the National Academy of Sciences. 2012; 109:2027.
8. Wang X, He L, Wu YI, Hahn KM, Montell DJ. Nature Cell Biology. 2010; 12:591. [PubMed: 20473296]
9. Berdahl A, Torney CJ, Ioannou CC, Faria JJ, Couzin ID. Science. 2013; 339:574. [PubMed: 23372013]
10. Lin B, Yin T, Wu YI, Inoue T, Levchenko A. Nature Communications. 2015; 6
11. Carmona-Fontaine C, Matthews HK, Kuriyama S, Moreno M, Dunn GA, Parsons M, Stern CD, Mayor R. Nature. 2008; 456:957. [PubMed: 19078960]
12. Desai RA, Gopal SB, Chen S, Chen CS. Journal of The Royal Society Interface. 2013; 10:20130717.
13. Simons AM. Trends in Ecology & Evolution. 2004; 19:453. [PubMed: 16701304]
14. Coburn L, Cerone L, Torney C, Couzin ID, Neufeld Z. Physical Biology. 2013; 10:046002. [PubMed: 23752100]
15. Friedl P, Locker J, Sahai E, Segall JE. Nature Cell Biology. 2012; 14:777. [PubMed: 22854810]
16. Aceto N, Bardia A, Miyamoto DT, Donaldson MC, Wittner BS, Spencer JA, Yu M, Pely A, Engstrom A, Zhu H, et al. Cell. 2014; 158:1110. [PubMed: 25171411]
17. Selmeczi D, Mosler S, Hagedorn PH, Larsen NB, Flyvbjerg H. Biophysical Journal. 2005; 89:912. [PubMed: 15951372]
18. Van Kampen, NG. Stochastic Processes in Physics and Chemistry. Vol. 1. Elsevier; 1992.
19. Mayor R, Carmona-Fontaine C. Trends in Cell Biology. 2010; 20:319. [PubMed: 20399659]
20. Camley BA, Zhang Y, Zhao Y, Li B, Ben-Jacob E, Levine H, Rappel W-J. Proceedings of the National Academy of Sciences. 2014; 111:14770.
21. Abercrombie M. Nature. 1979; 281:259. [PubMed: 551275]
22. Kim, S.; Karrila, SJ. Microhydrodynamics: principles and selected applications. Courier Dover Publications; 2013.
23. Han Y, Alsayed A, Nobili M, Zhang J, Lubensky TC, Yodh AG. Science. 2006; 314:626. [PubMed: 17068256]
24. Fuller D, Chen W, Adler M, Groisman A, Levine H, Rappel W-J, Loomis WF. Proceedings of the National Academy of Sciences. 2010; 107:9656.
25. Angelini TE, Hannezo E, Trepat X, Fredberg JJ, Weitz DA. Physical Review Letters. 2010; 104:168104. [PubMed: 20482085]
26. Angelini TE, Hannezo E, Trepat X, Marquez M, Fredberg JJ, Weitz DA. Proceedings of the National Academy of Sciences. 2011; 108:4714.
27. Szabó A, Ünnep R, Méhes E, Twal W, Argraves W, Cao Y, Czirók A. Physical Biology. 2010; 7:046007. [PubMed: 21076204]
28. Vedula SRK, Ravasio A, Lim CT, Ladoux B. Physiology. 2013; 28:370. [PubMed: 24186932]
29. Warren P. Physical Review E. 2003; 68:066702.
30. Amselem G, Theves M, Bae A, Bodenschatz E, Beta C. PloS ONE. 2012; 7:e37213. [PubMed: 22662138]
31. Levchenko A, Iglesias PA. Biophysical Journal. 2002; 82:50. [PubMed: 11751295]
32. Takeda K, Shao D, Adler M, Charest PG, Loomis WF, Levine H, Groisman A, Rappel W-J, Firtel RA. Science Signaling. 2012; 5:ra2. [PubMed: 22215733]
33. Sepúlveda N, Petitjean L, Cochet O, Grasland-Mongrain E, Silberzan P, Hakim V. PLoS Computational Biology. 2013; 9:e1002944. [PubMed: 23505356]
34. Camley BA, Rappel W-J. Physical Review E. 2014; 89:062705.

35. Szabo B, Szöllösi G, Gönci B, Jurányi Z, Selmeczi D, Vicsek T. Physical Review E. 2006; 74:061908.
36. Li B, Sun SX. Biophysical Journal. 2014; 107:1532. [PubMed: 25296305]
37. Czirók A, Ben-Jacob E, Cohen I, Vicsek T. Physical Review E. 1996; 54:1791.
38. van Drongelen R, Pal A, Goodrich CP, Idema T. Physical Review E. 2015; 91:032706.
39. Basan M, Elgeti J, Hannezo E, Rappel W-J, Levine H. Proceedings of the National Academy of Sciences. 2013; 110:2452.
40. Zimmermann J, Hayes RL, Basan M, Onuchic JN, Rappel W-J, Levine H. Biophysical Journal. 2014; 107:548. [PubMed: 25099794]
41. Segerer FJ, Thüroff F, Alberola AP, Frey E, Rädler JO. Physical Review Letters. 2015; 114:228102. [PubMed: 26196648]

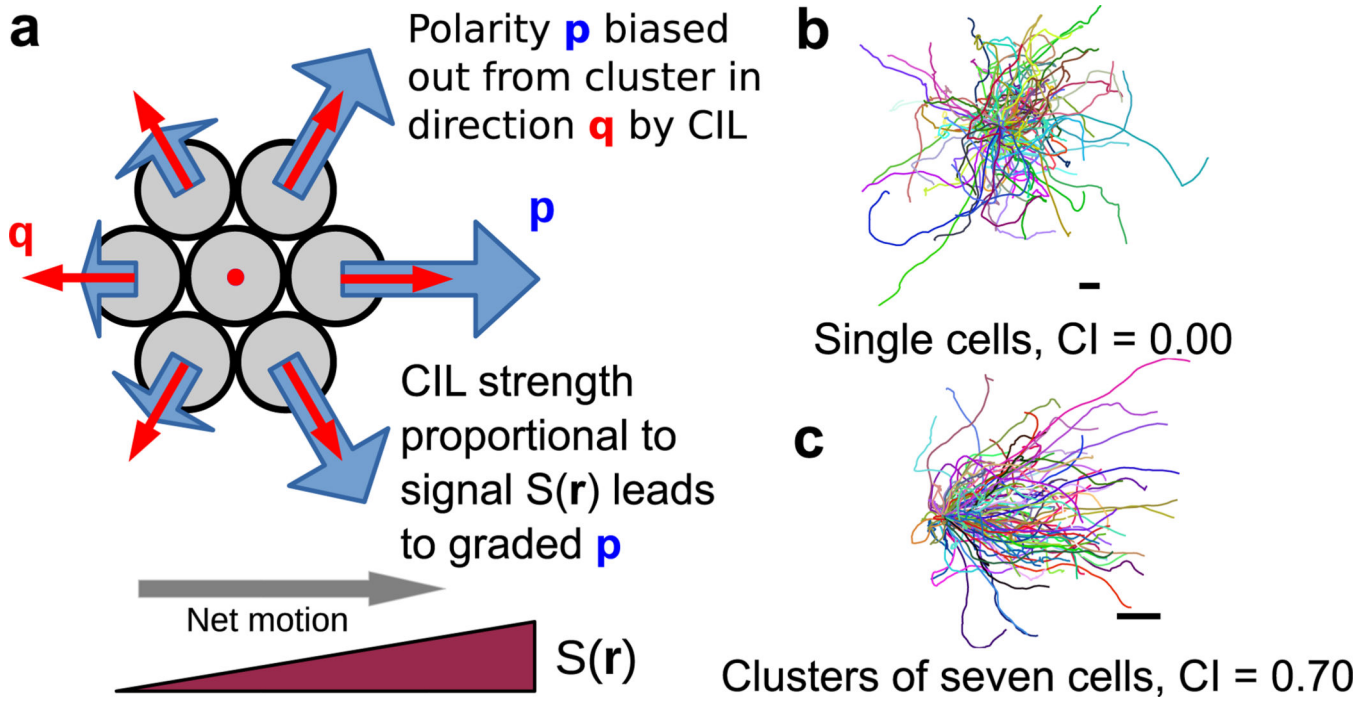

FIG. 1. Signal-dependent contact inhibition of locomotion creates directed motion

a, Schematic picture of model and origin of directed motion. Cell polarities are biased away from the cluster toward the direction $\mathbf{q}^i = \sum_{j\sim i} \mathbf{r}^{\hat{ij}}$ by contact inhibition of locomotion (CIL); the strength of this bias is proportional to the local chemoattractant value $S(\mathbf{r})$, leading to cells being more polarized at higher S. See text for details. **b**, One hundred trajectories of a single cell and **c**, cluster of seven cells. Trajectories are six persistence times in length (120 min). Scalebar is one cell diameter. Gradient strength $|\nabla S| = 0.025$, with the gradient in the x direction.

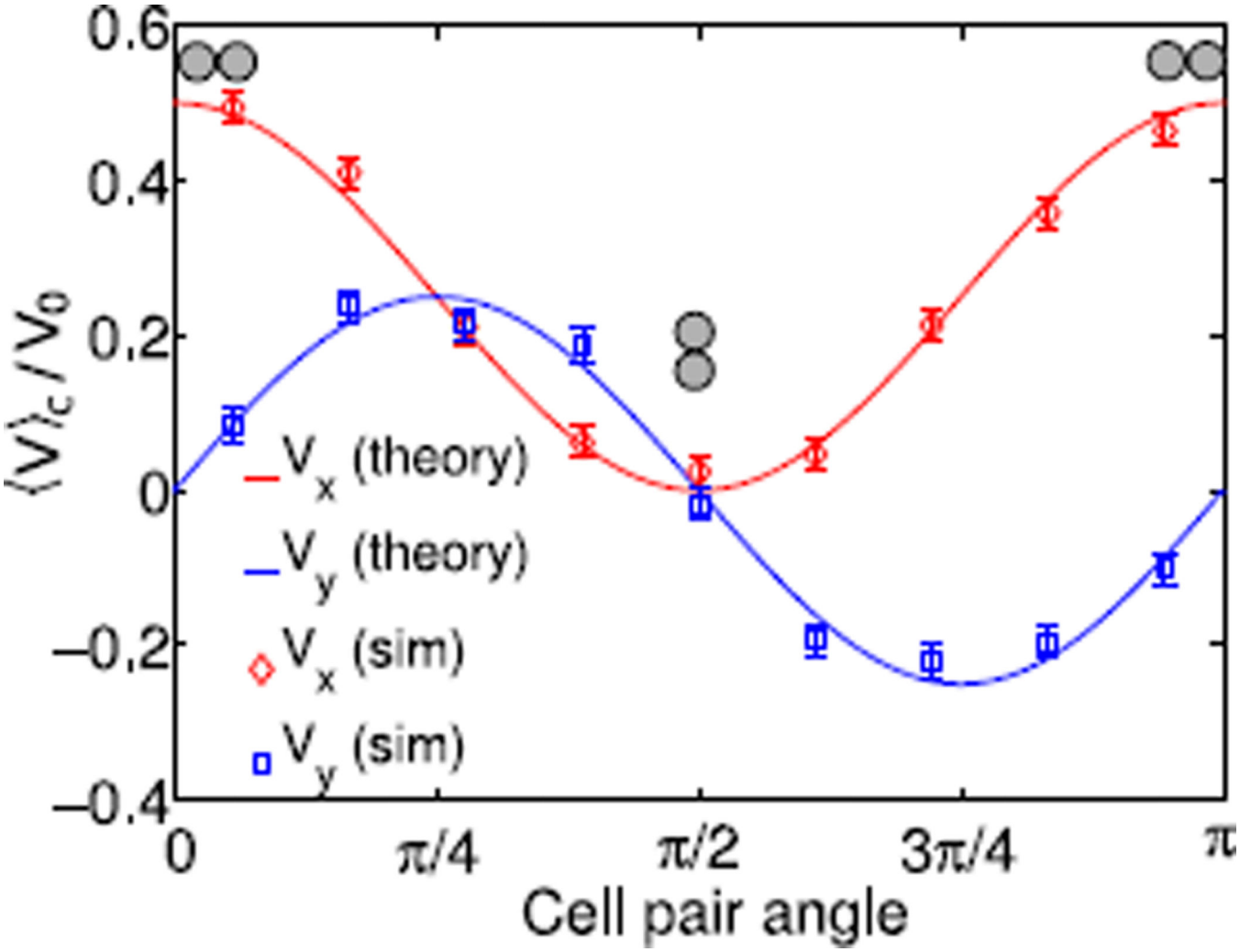

FIG. 2. Adherent pairs of cells undergo highly anisotropic chemotaxis

The average chemotactic velocity of a cell pair $\langle V_x \rangle_c$ depends strongly on the angle θ between the cell-cell axis and the chemotactic gradient. Cell pairs also drift perpendicular to the gradient, $\langle V_y \rangle_c \neq 0$. $V_0 \equiv \beta\bar{\tau}|\nabla S|$ is the velocity scale; $|\nabla S| = 0.025$. Simulations are of Eqs. 1–2. We compute $\langle V_\mu \rangle_c$ by tracking the instantaneous angle, then averaging over all velocities within the appropriate angle bin. Error bars here and throughout are one standard deviation of the mean, calculated from a bootstrap. Over $n = 13,000$ trajectories of $6\bar{\tau}$ (120 minutes) are simulated.

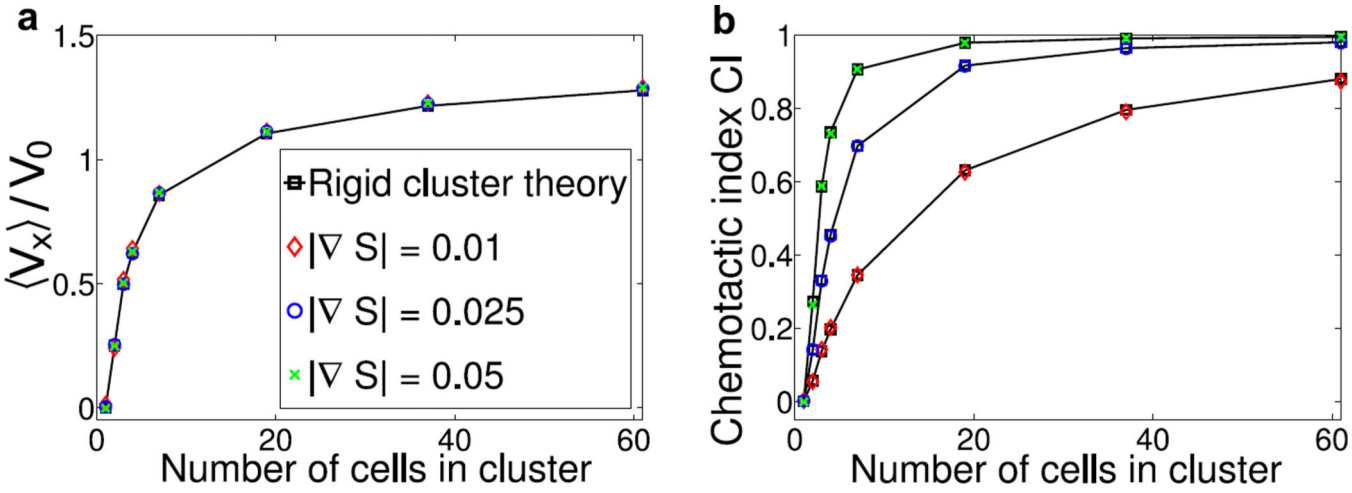

FIG. 3. Larger cell clusters chemotax more effectively, but their velocity saturates

a, As the number of cells N in a cluster increases, the mean velocity $\langle V_x \rangle$ increases with N but then saturates; the mean velocity can be collapsed onto a single curve by rescaling by $V_0 \equiv \beta\bar{\tau}|\nabla S|$. **b**, The chemotactic index CI also saturates to its maximum value. Black squares and lines are the orientationally-averaged drift velocity computed for rigid clusters by Eq. 3 and Eq. 6. Colored symbols are full model simulations with strong adhesion. Cell cluster shape may influence $\langle V_x \rangle$ (*Supplementary Information* Fig. S4); our calculations are for the shapes in Table S1. Error bars here are symbol size or smaller; $n \geq 2000$ trajectories of 6τ are used for each point.

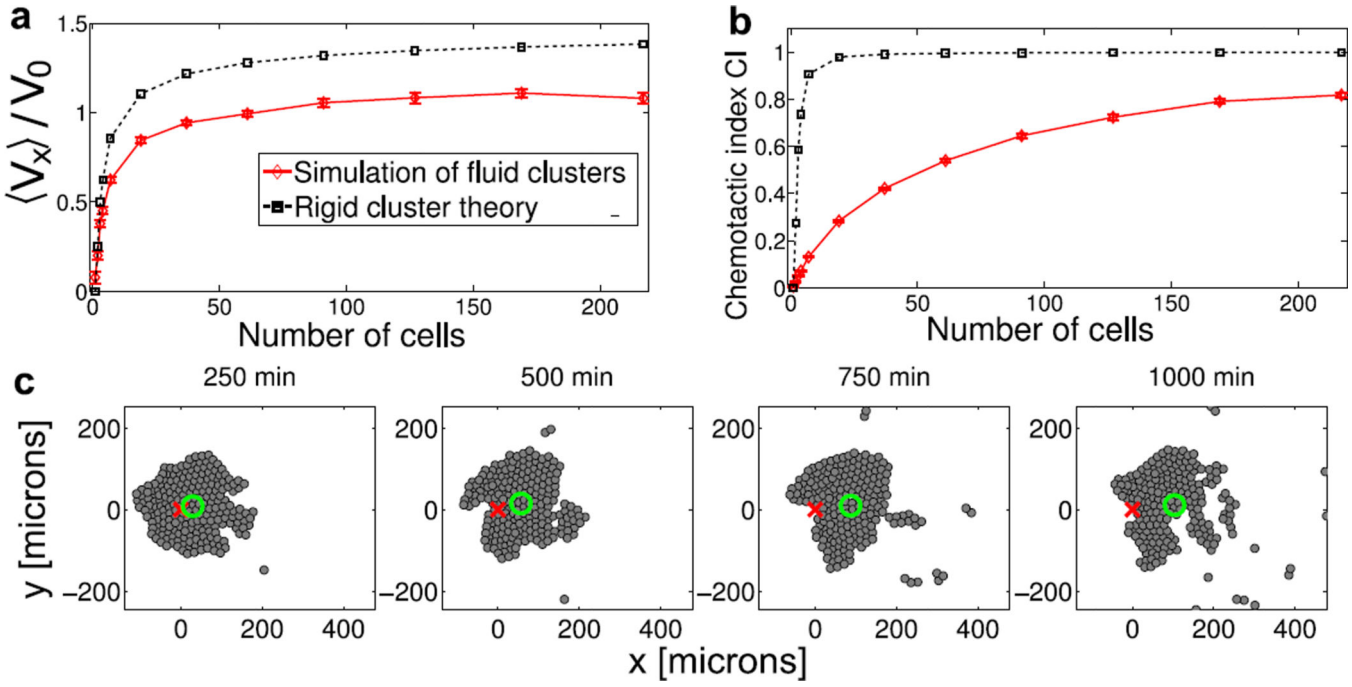

FIG. 4. Nonrigid clusters may also chemotax via collective guidance

a, As the number of cells N in a cluster increases, the mean velocity $\langle V_x \rangle$ increases with N but then saturates. **b**, Chemotactic index approaches unity, but slower than in a rigid cluster. Rigid cluster theory assumes the same cluster geometries as in Fig. 3. Averages in **a–b** are over $n \geq 20$ trajectories (ranging from $n = 20$ for $N = 217$ to $n = 4000$ for $N = 1, 2$), over the time 12.5τ to 50τ. **c**, Breakdown of a cluster as it moves up the chemoattractant gradient. X marks the initial cluster center of mass, O the current center. $|\nabla S| = 0.1$, $\bar{\beta} = 1$ in this simulation.